Packings of monodisperse emulsions in flat microfluidic channels

Ohle Claussen, Stephan Herminghaus, and Martin Brinkmann*
Max-Planck Institute for Dynamics and Self-Organization, Bunsenstrasse 10, 37073 Göttingen, Germany
(Received 24 November 2010; revised manuscript received 18 February 2012; published 6 June 2012)

In the lateral confinement of a flat microfluidic channel, monodisperse emulsion droplets spontaneously self-organize in a variety of topologically different packings. The explicit construction of mechanically equilibrated arrangements of effectively two-dimensional congruent droplet shapes reveals the existence of multiple mechanical equilibria depending on channel width W, droplet area A_d, and volume fraction ϕ of the dispersed phase. The corresponding boundaries of local or global stability are summarized in a packing diagram for congruent droplet shapes in terms of the dimensionless channel width $w = W/\sqrt{A_d}$ and ϕ. In agreement with experimental results, an increasingly strong hysteresis of the transition between single-row and two-row packings is observed during changes of w above a threshold volume fraction of $\phi^* \simeq 0.813$.

DOI: 10.1103/PhysRevE.85.061403 PACS number(s): 83.80.Iz, 47.57.Bc

I. INTRODUCTION

Microfluidic systems allow the production of monodisperse emulsions with controlled droplet volume and volume fraction at high rates [1,2]. Under proper conditions these emulsions can be stable in the confinement of a microchannel on a time scale of several hours to days [3]. The coalescence of neighboring droplets can be largely suppressed by suitable surfactant molecules [3] or even by macroscopic particles that adsorb to the liquid-liquid interface [4]. This astonishing stability against coalescence allows one to employ, for example, individual emulsion droplets as tiny mobile containers for living cells in microbiological applications [5,6] or as chemical reactors on the micrometer scale [7]. Manipulations of flowing droplets, such as the merging of two adjacent droplets triggered by an electric pulse [8] or active sorting into different channels [9], open a large range of applications. The ability to control the packing geometry of static emulsions in confinement is relevant in microfluidic applications where the neighboring relations of individual droplets are essential [10].

In this work we present a theoretical study on the appearance and stability of regular droplet packings in flat rectangular microfluidic channels. Because the diameter of the emulsion droplets is typically on the order of the channel dimensions, the emulsion droplets spontaneously arrange in a variety of topologically different packings once the volume fraction of the dispersed phase exceeds a certain value. In the absence of external forces the entire arrangement process is driven by interfacial energy. Changes in the two control parameters, i.e., volume fraction and channel width, induce transitions between topologically different droplet packings.

A large impact of the volume fraction on the appearance and stability of certain droplet and particle packings in confinement has been reported in a number of microfluidic experiments [11–15]. Transitions between single-row, two-row, and three-row packings of monodisperse emulsion droplets in tapered channels have been described in detail by Surenjav *et al.* in Ref. [14]. In their experimental setup the droplets are slowly compressed or decompressed while flowing down a microfluidic channel of linearly varying width. At low volume fractions of the dispersed phase, the transition from a single-row to a two-row structure and the inverse transition occur at the same channel width. Above a certain volume fraction, however, the transitions in the widening segment occur at a larger channel width than the inverse transition, i.e., an increasing hysteresis of the transitions is observed that eventually reaches the strong hysteresis observed in dry emulsions [14]. Using plugs of a fluorinated oil that is immiscible to both the droplet and the continuous phases allows one to compress a stack of droplets in a flat microfluidic channel and to study packing transitions [15]. Besides transitions between congruent droplet arrangements, a longitudinal separation into packings with high and low packing fractions is observed in a certain range of confinement and volume fraction [15].

The hysteresis of transitions between different static and flowing foam packings in flat microfluidic channels has been investigated both experimentally [16,17] and in computer simulations employing the viscous froth model [16,18]. Hysteretic transitions between ordered packings have also been reported for monodisperse dry foams in tubes with cylindrical [19] and rectangular [20] cross sections during compression and decompression cycles. In recent experiments Raven and Marmottant [17,21] considered wet foams flowing in rectangular channels, where they found a hysteretic transition from single- to two-row packings controlled by the gas pressure and the flow rate of the continuous phase.

Motivated by the experiments described in Ref. [14], we computed the packing geometry of mechanically equilibrated droplet arrangements in flat and straight microchannels of a rectangular cross section for a given droplet size and volume fraction of the dispersed phase. Provided effects of viscous dissipation are negligible, our results should also apply to slowly flowing emulsions. Regarding monodisperse foams of micrometer-sized bubbles instead of emulsions, the dispersed gas phase can be safely treated as a virtually incompressible fluid. If, in addition, the diffusion of gas molecules between adjacent bubbles is sufficiently slow, it is justified to consider the bubble volume as a proper control parameter. Under these conditions the mechanical stability of a foam and an emulsion for the same packing geometry should be identical.

*Present address: Saarland University, Experimental Physics, D-66041 Saarbrücken, Germany; martin.brinkmann@ds.mpg.de

This article is organized as follows. In Sec. II we will introduce a description of effectively two-dimensional packings of emulsion droplets in linear microchannels. The appearance of certain classes of periodic arrangements of congruent droplets in the channel is summarized in a packing diagram in Sec. III. In Sec. IV we discuss the hysteretic transitions between different packings of congruent droplets. A summary and outlook are given in Sec. V. The explicit construction of effectively two-dimensional droplet packings from purely geometric considerations is explained in the Appendixes.

II. PHYSICAL MODEL

In a typical microfluidic setup the exchange of solvent molecules between the dispersed phase and the continuous phase is slow on experimentally relevant time scales. Hence we will neglect coarsening of the emulsion droplets by diffusion in the following considerations. In this situation each mechanically stable droplet packing corresponds to a local minimum of the interfacial energy for a given droplet volume V_d and volume fraction of the dispersed phase ϕ.

By use of the Laplace law $\Delta P \equiv P_d - P_c = 2M\gamma$, we can relate the local mean curvature M and interfacial tension γ of the liquid-liquid interface to the difference between the pressure P_d inside a droplet and the pressure P_c of the continuous phase at a particular point of the interface. Spatial variations of ΔP due to hydrostatic pressure contributions are negligible since we assume the dimensions of the cross section of the channels to be small compared to the capillary length $L_c = \sqrt{\gamma/g|\Delta\rho|}$, where $\Delta\rho$ is the density difference between the liquid phases and g is the acceleration of gravity. Moreover, we assume a chemical equilibrium of surfactant molecules and hence discard spatial variations of the interfacial tension. Under these assumptions any interface between the dispersed liquid and the continuous phase will be a surface of constant mean curvature in mechanical equilibrium.

In this work we will consider packings of monodisperse emulsion droplets confined to straight, flat channels of rectangular cross section and restrict our analysis to periodic packings composed of congruent droplets. In other words, the channel can be tiled by use of a single droplet shape only. This assumption implies that each droplet will have the same pressure P_d in mechanical equilibrium. Besides the droplet volume V_d, each packing is characterized by the volume of the continuous phase in a tile V_c. The volume fraction of the dispersed phase ϕ can thus be expressed by $\phi = V_d/(V_d + V_c)$.

A. Stability

In certain ranges of the control parameter droplet volume V_d and volume fraction of the dispersed phase ϕ, the geometrical construction of congruent droplet packings allows for multiple equilibrium configurations. The stability of these equilibria, however, is not obvious and some of the solutions will correspond to mechanically unstable packings.

In this work we will infer stability from the complete set of equilibrium configurations for given values of the control parameter. Any mechanically equilibrated droplet packing represents either a local minimum of the interfacial energy or a saddle point in the energy landscape under the constraint of a fixed volume. In a complete set of mechanical equilibria, the configuration with the lowest interfacial energy must be mechanically stable, while the configuration with the highest interfacial energy must correspond to an unstable saddle point.

In the present study we impose the constraints of constant droplet volume and congruency of droplet shapes. Releasing the system from one of these constraints or both can transform a local minimum of the energy landscape into a saddle point, i.e., the packing may become unstable. As we consider packings of congruent droplets, there is always the possibility that such a packing is unstable with respect to perturbations that do not preserve the congruency of the tiles. Indeed, the instability of certain congruent droplet packings with respect to longitudinal variations of the packing fraction is observed both in microfluidic experiments and in numerical minimizations of the interfacial energy [15].

Information about the local stability of a droplet packing with respect to arbitrary small perturbations can, in principle, be obtained from a spectral analysis of the second variation of the interfacial energy. Such a stability analysis has been applied to predict the stability of liquid droplets in contact with structured surfaces [22,23].

B. Effectively two-dimensional model

In flat channels, i.e., where the ratio of channel height D to channel width W is small compared to unity, droplets with volumes $V_d \gg D^3$ assume pancakelike, effectively two-dimensional shapes. This situation is sketched in Fig. 1(a). On the one hand, the radius of curvature R of the free in-plane droplet contour, i.e., those parts of the contour that are not in contact with either the channel wall or another droplet, will be much larger than the height of the channel. On the other hand,

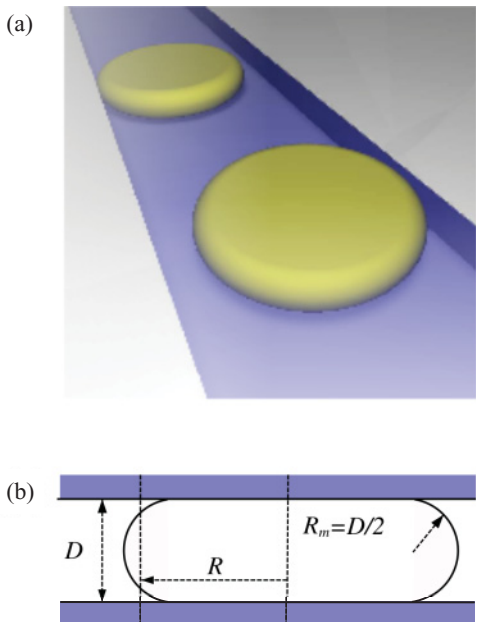

FIG. 1. (Color online) (a) Three-dimensional illustration of a flat, pancakelike droplet confined in a rectangular channel with an invisible top plate. (b) Cross section through such a droplet. Here R is the radius of the effective droplet contour and $R_m = D/2$ denotes the radius of the meniscus.

the out-of-plane contour of the meniscus can be approximated by a segment of a cylindrical torus with radius $R_m = D/2 \ll R$ [see Fig. 1(b)]. This separation of length scales allows us to write the mean curvature M of the liquid-liquid interface as the sum

$$2M = C_\perp + \nu\, C_\parallel + O\left(\frac{D}{R^2}\right), \tag{1}$$

with the leading order of the out-of-plane curvature of the liquid-liquid interface $C_\perp = 2/D$ and the in-plane curvature of the droplet contour $C_\parallel = 1/R \ll C_\perp$. The numerical prefactor ν is not identical to one, as one may naively expect, but assumes the value of $\pi/4$ for perfectly nonwetting conditions, i.e., in the case where the dispersed phase forms a contact angle $\theta = \pi$ with the channel walls. The numerical prefactor will be explained later in this section. Throughout this work we will assume perfectly nonwetting conditions for the dispersed phase on the channel walls, which is the usual case in droplet-based microfluidics, where surfactants are used to prevent the merging of droplets.

According to the law of Laplace and the mean curvature of the liquid-liquid interface [Eq. (1)], we may write the Laplace pressure of a droplet as the sum

$$\Delta P = \Delta P_\perp + \Delta P_\parallel \tag{2}$$

of a constant pressure offset $\Delta P_\perp = 2\gamma/D$ and a contribution

$$\Delta P_\parallel = \frac{\pi\gamma}{4R} + O\left(\frac{\gamma D}{R^2}\right), \tag{3}$$

which depends solely on the radius of curvature R of the contact line between the continuous and dispersed phases. The pressure contribution $\Delta P_\parallel$ can be viewed as the two-dimensional analog to the Laplace pressure in three dimensions because it relates to the in-plane curvature of a two-dimensional droplet. In contrast, the pressure $\Delta P_\perp$ depends only on the vertical confinement.

The prefactor of $\pi/4$ of the in-plane curvature in Eq. (1) can be rationalized from the limiting process mapping a three-dimensional droplet packing to the purely two-dimensional model. In the asymptotic limit $D/W \to 0$ of an ideal two-dimensional system, one may consider the area enclosed by the droplet contour instead of its volume. Hence the reference position of the in-plane contour of a three-dimensional droplet must be chosen such that the area A_d enclosed by the contour and the droplet volume V_d satisfy $A_d = V_d/D + O(L^0)$, where L is the length of the droplet perimeter. This procedure is similar to the construction of the Gibbs dividing surface between a coexisting vapor and liquid phase of a single-component fluid.

Figure 1(b) displays the position of the effective droplet contour by the left vertical line. This line cuts the meniscus such that the area of the dispersed phase on the left side equals the area of continuous phase on the right side. Referring to this effective in-plane contour, the interfacial energy E can be written as the sum

$$E = 2\gamma A_d + \tau L + O(L^0), \tag{4}$$

where

$$\tau = \frac{\pi\gamma D}{4} \tag{5}$$

represents the interfacial energy of the meniscus per unit length of the effective contour. For a circular droplet it can be checked by an explicit calculation that the derivative of the interfacial energy (4) with respect to the volume directly yields the Laplace pressure (2) and hence a prefactor of $\nu = \pi/4$ in Eq. (1).

Due to the finite lateral extension of the meniscus, the distance between the effective contours of two droplets in mutual contact may not be smaller than a minimal separation of $S_{\min} = (1 - \pi/4)D$. In the asymptotic limit $D/R \to 0$, however, the effect of the finite separation between two effective droplet contours becomes negligible. Together with the observation that congruent droplets in a mechanically equilibrated packing have the same pressure, this implies the following set of construction rules for effectively two-dimensional congruent packings: (i) The contour of a droplet is straight at points where it touches one of its neighboring droplets, (ii) the curved parts of the contour bounding the droplet to the continuous phase have the same curvature, (iii) segments of the contour in contact with the lateral channel walls are described by straight lines (as long as the channel walls are straight), and (iv) the contour is smooth at every point (the normal to the contour is continuous).

Throughout the rest of this paper we will speak of *effectively two-dimensional droplets*, meaning such droplets where the vertical confinement of the microfluidic channel allows us to factor out the contributions of the out-of plane curvature, as above. As we are working exclusively in the asymptotic limit of flat channels, we will from now on use the term area fraction for ϕ instead of volume fraction and characterize flat droplets by the effective area $A_d \equiv V_d/D$ of the droplets. In a truly two-dimensional system the term continuous phase is misleading since the continuous phase is separated into disconnected compartments by the droplet phase. As mentioned previously, the continuous phase in a real three-dimensional system communicates via thin plateau borders at the channel walls and the pressure of the continuous phase becomes identical in all compartments in mechanical equilibrium.

III. DROPLET PACKINGS

Employing elementary geometry, we are able to construct a number of effectively two-dimensional packings of congruent droplet shapes that satisfy the geometrical equilibrium conditions given in Sec. II. Figure 2(a) displays possible packings in a strip of constant width. Each packing geometry is characterized by the topology of its contact network, which is defined by mutual droplet contacts and contacts of droplets with the sidewalls.

The appearance and stability of the droplet packings shown in Fig. 2(a) at a given droplet size and area fraction is best illustrated in the form of a packing diagram. Figure 2(b) shows the packing diagram for congruent droplet packings in flat channels in terms of the dimensionless channel width $w \equiv W/\sqrt{A_d}$ and area fraction of the dispersed phase ϕ. Alternatively to the dimensionless channel width w, we will employ the dimensionless droplet area $a_d \equiv A_d/W^2 = 1/w^2$ in our calculations. Dimensionless rescaled quantities will be denoted by lowercase letters.

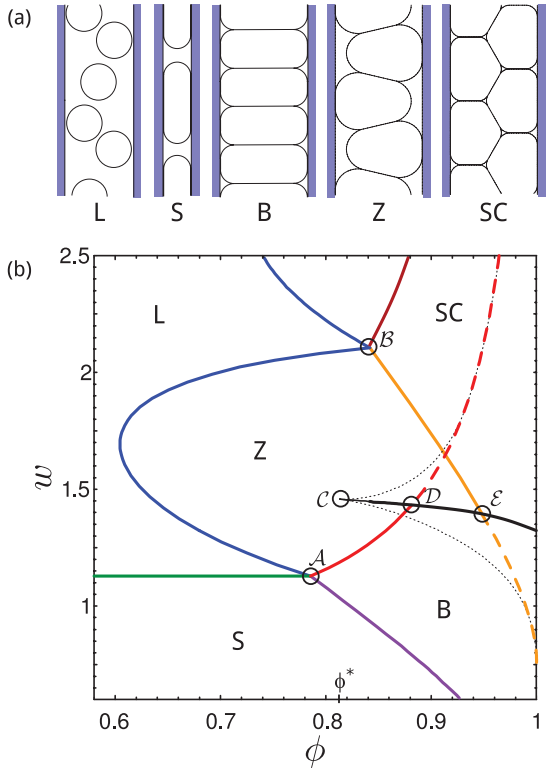

FIG. 2. (Color online) (a) Different packings of monodisperse effectively two-dimensional droplets in a straight channel. From left to right: loose assembly (L), slugs (S), bamboo packing (B), zigzag packing with two neighbors (Z), and staircase packing (SC) with four neighbors. (b) Packing diagram of effectively two-dimensional monodisperse emulsion droplets in a rectangular channel geometry. The packing diagram is spanned by the following control parameters: area fraction ϕ and dimensionless channel width $w \equiv W/\sqrt{A_d}$. The colored lines represent continuous transitions between different droplet shapes. A solid line becoming dashed means that from this point on a further, third packing represents the global energy minimum. The dotted black lines mark the area where multiple solution branches exist. The circled points marked $\mathcal{A}$, $\mathcal{B}$, $\mathcal{C}$, $\mathcal{D}$, and $\mathcal{E}$ serve only as markers referred to in the text.

In the packing diagram Fig. 2(b), each of the constructed packings is mapped onto a corresponding region of the control parameters w and ϕ, where this particular packing is found to be a mechanically stable state or even represents the global minimum of the interfacial energy. Solid lines in the diagram indicate the sets of points where the global minimum changes between two packing geometries. We will refer to these lines as transition lines.

In principle, two types of transition lines can be distinguished. On the first type of transition line the global minimum changes continuously between two topologically distinct packing geometries and a continuous transformation of the droplet shapes is observed. On the second type of transition line, however, two droplet configurations with the same minimal energy are found, which are separated by an energy barrier. For the latter type, we find regions of metastability for the particular packing, which represents the global energy minimum on the opposite side of the transition line.

Sets of points in the packing diagram [Fig. 2(b)] where local energy minima corresponding to a certain packing geometry cease to exist are indicated by dotted lines. Crossing a dotted line leads to a discontinuous change in the droplet configuration of this droplet packing. Hence we will refer to this type of line as a boundary of mechanical stability. Besides transition lines and boundaries of mechanical stability, the packing diagram includes a third type of line: Dashed lines display the sets of points where a metastable droplet packing transforms continuously into another metastable packing geometry.

The explicit construction of packings of congruent droplets allows us to compute all lines in the packing diagram [Fig. 2(b)] analytically. In the remainder of this section we will present and discuss the results of our calculations. Details of the computation are provided in Appendix A.

At low area fractions ϕ and for small confinements w each droplet is in contact with both channel walls and is separated by equal amounts of the continuous phase [see also the sketch in Fig. 2(a)]. In the following we will refer to these droplets as slugs (abbreviated by S in the figure). As the area fraction of the dispersed phase is increased at a constant confinement, these slug-shaped droplets will eventually touch each other. Hence the region of slugs in the packing diagram Fig. 2(b) is bounded by two curves: If the area fraction satisfies $\phi \leqslant \pi/4$, the droplets first experience the lateral confinement of the channel and will transform into slugs once $w \leqslant 2/\sqrt{\pi}$. In the packing diagram Fig. 2(b) this transition is indicated by the horizontal solid (green) line ending at point $\mathcal{A}$. For fixed area fractions $\phi \geqslant \pi/4$, two neighboring slugs will first touch each other as w is increased before losing contact with both channel walls. In the particular configuration where the slug touches its neighbors in just a single point, the continuous phase in a tile occupies that area within the unit square around the contact point that is not covered by the two half circles of the slugs (i.e., an inverse unit circle), so that the transition is characterized by a dimensionless channel width

$$w = 2\sqrt{\frac{1-\phi}{(4-\pi)\,\phi}}, \tag{6}$$

as indicated by the purple line at the bottom of Fig. 2(b), starting from point $\mathcal{A}$ and moving to smaller channel widths. When crossing this line toward larger channel widths w, two neighboring droplets form a straight lamella with an orientation perpendicular to the channel. Due to its characteristic shape, resembling a stack of rounded rectangles, the latter structure has been termed a bamboo structure and will be abbreviated B.

When increasing the area fraction ϕ of a loose assembly of droplets with a diameter slightly smaller than the channel width, the droplets will arrange in a zigzaglike geometry [see also the sketch marked Z in Fig. 2(a)]. In this packing each droplet is in contact with two neighboring droplets and with one side of the channel wall. The area fraction of dispersed phase at this jamming transition corresponds to the densest regular packing of nonoverlapping circular disks between two parallel lines. However, we cannot rule out the existence of mechanically stable droplet packings below this value of ϕ.

It is widely accepted (but not strictly proven) that packings built out of triangular domains of hexagonally close-packed

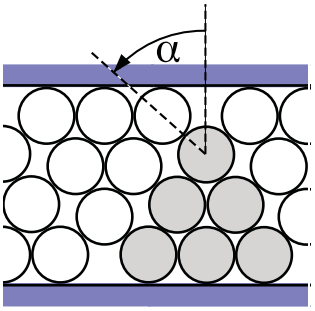

FIG. 3. (Color online) Ideal triangular domain packing of monodisperse circular droplets. In this example the angle α parametrizes packings between a three-row packing at $\pi/2$ and a four-row packing at $\pi/6$. The dimensionless channel width w and the area fraction ϕ are given by Eqs. (7) and (8), respectively. For the case shown here, the number of perfect rows in the triangular domain is $n = 3$.

circular disks with alternating orientation represent the densest packing in a parallel strip [24,25] (see also Fig. 3). In Ref. [25] Füredi gave a proof for a strip width in the range $(2+\sqrt{3})/\sqrt{\pi} \leqslant w \leqslant (2+2\sqrt{3})/\sqrt{\pi}$, i.e., for packings between two and three rows of perfect hexagonal disk arrangements. In strips with a width of $2/\sqrt{\pi} \leqslant w \leqslant (2+\sqrt{3})/\sqrt{\pi}$, circular disks can be arranged into a zigzag packing where each disk touches two neighboring disks and either one or the other sidewall of the channel.

In the packing diagram shown in Fig. 2(b), triangular domain packings of circular disks are found on the solid (blue) line between points $\mathcal{A}$ and $\mathcal{B}$ and the solid (blue) line starting from $\mathcal{B}$ toward smaller ϕ and larger w. These curves are parametrized by

$$w = \frac{2+\sqrt{3}(n-1)+2\cos\alpha}{\sqrt{\pi}} \tag{7}$$

and

$$\phi = \frac{\pi n(n+1)}{[2\,(n-1)+4\sin\alpha][2+\sqrt{3}(n-1)+2\cos\alpha]}, \tag{8}$$

where n is the number of rows in a triangular domain and $\alpha \in [\pi/6,\pi/2]$ is a packing angle. For assemblies of effectively dimensional droplets in a microchannel, this line should correspond to a transition between a loose packing and a compressed packing.

Note that Eqs. (8) and (7) yield identical values for $(n,\alpha = \pi/6)$ and $(n+1,\alpha = \pi/2)$ and hence define a continuous curve in the space of the control parameter. Each kink in the transition line corresponds to a perfect hexagonal disk packing of n layers. Upon increasing the dimensionless channel width w, the transition line bows to lower packing fractions ϕ between two subsequent kinks.

Upon crossing the lowest bow of the transition line, i.e., the part between points $\mathcal{A}$ and $\mathcal{B}$, a loose disk assembly transforms into a zigzag structure during an increase of the area fraction ϕ. We will refer to this packing as the zigzag packing Z, which can be regarded as a special case of a triangular domain packing compressed beyond the jamming line. Similar to the triangular domain packings, a zigzag packing is characterized by the angle α between the channel wall and the lamella separating two adjacent droplets [see Fig. 2(a)]. In the region at higher area fractions enclosed by the second bow we expect to find three-row structures. However, these structures do not belong to the class of packings composed of congruent droplet shapes.

In the asymptotic limit of a completely dry emulsion, i.e., for an area fraction $\phi \to 1$, we find packings where each droplet is in contact with four neighboring droplets. Owing to the particular shape of the droplets, we will refer to this structure as the staircase packing SC [see Fig. 2(a)]. Consequently, there must be a transition between the zigzag packing with two neighbors and the staircase packing with four neighbors at a certain value of the area fraction.

According to the equilibrium conditions for effectively two-dimensional droplet packings in Sec. II, the lamella angle of the staircase structure is fixed to $\alpha = \pi/6$ in mechanical equilibrium (see also Fig. 6 in Appendix A). This implies that the dimensionless channel width of a packing SC cannot become smaller than $w = 3^{-1/4} \simeq 0.7598$ in the dry limit $\phi \to 1$. For dimensionless channel widths $w < 3^{-1/4}$ we find the bamboo structure as the only mechanically stable droplet configuration in the dry limit. This implies that we will observe a transition from a zigzag structure to a bamboo structure during an increase of the area fraction of the dispersed phase in sufficiently narrow channels.

A similar symmetry-breaking transition has been described for a dry foam in a similar geometry by Fortes *et al.* [26]. In the latter case a pair of effectively two-dimensional twin bubbles in contact with two confining parallel straight walls undergoes a buckling transition upon a decrease of the wall to wall distance. Predicted by an analytical model and confirmed by experiments, the lamella shared by the twin bubbles is oriented parallel to the confining walls for sufficiently large distances. Below a certain distance the lamella becomes tilted with respect to the orientation of the confining walls. In contrast to the transition between bamboo and zigzag packing in our analysis, the buckling transition of the twin bubble is always continuous.

The brown line in Fig. 2(b), starting at $\mathcal{B}$ towards higher area fractions and channel widths, marks the parameters where the contour length of a droplet in an SC packing that is in contact with the channel wall becomes zero. On this line droplets touch the sidewall only at a single point. This transition is similar to that between packings of types Z and B. For the region above this line, no congruent two-row packing can be constructed.

The explicit construction of equilibrium configurations allows us to compute the transition line between packings Z and B in the form of a parametric curve, which is displayed by the red line in the packing diagram in Fig. 2(b), going from $\mathcal{A}$ to $\mathcal{D}$ and continuing as a dashed line beyond $\mathcal{D}$. On this transition line we find configurations Z whose lamella angle α has reached $\pi/2$ from below. These configurations can also be regarded as a bamboo packing, where each droplet touches both sidewalls at a single point.

For sufficiently small droplet area or, equivalently, a large channel width, however, a transition of Z directly into a staircase packing is observed. Along the corresponding transition line we find configurations Z where the contour of two next-nearest-neighbor droplets touches in a single point.

The transition line can be expressed by a parametric curve, which is displayed as the yellow line in Fig. 2(b), starting at $\mathcal{B}$.

The explicit construction of the packings Z, SC, and B reveals that multiple equilibrium configurations exist in a certain range of control parameters. In the present system we find either one or three equilibrium configurations of congruent droplet shapes for given values of the dimensionless channel width w and area fraction ϕ for dry emulsions. The two solutions with the lowest energies represent mechanically stable configurations. The remaining configuration with the highest interfacial energy corresponds to a saddle point in the energy landscape and hence is mechanically unstable.

Crossing the boundaries of mechanical stability indicated by the (black) dotted lines in Fig. 2(b), the unstable configuration and one of the other two mechanically stable configurations merge with the saddle point configuration and disappear. The global minimum of the interfacial energy changes between the two mechanically stable configurations along the solid (black) line, which ends together with the two dotted lines at a cusp with $\phi = \phi^* \simeq 0.8130$ and $w = w^* \simeq 1.458$ (point $\mathcal{C}$). Calculations of the lines bounding the region of mechanical stability of the metastable zigzag packing and of the bifurcation point at the tip of the cusp are explained in Appendix B.

In the immediate vicinity of the cusp between points $\mathcal{C}$ and $\mathcal{D}$ we find a transition between two zigzag packings with different packing angle α. Beyond point $\mathcal{D}$, the (black) line continues as a transition line between the remaining mechanically stable zigzag packing and the bamboo packing until, at even larger area fractions, this transition line crosses the continuous transition line between the remaining mechanically stable zigzag packing and the staircase packing at $\mathcal{E}$. As expected, the last part of the (black) transition line corresponds to a transition between bamboo and zigzag packings.

IV. HYSTERESIS

The transitions and instabilities of droplet packings shown in the packing diagram in Fig. 2(b) can be exemplified in a series of plots of the dimensionless interfacial energy $e \equiv E/\tau W$ as a function of the dimensionless channel width w for fixed values of the area fraction ϕ (see Fig. 4). By construction of the effective droplet contour and because the area A_d of a droplet is constant we may drop the first term of the interfacial energy in Eq. (4). Owing to the explicit construction of the droplet packings outlined in Appendix A, we are able to express the dimensionless interfacial energy e of the droplets and the dimensionless channel width w as functions of a suitable parameter. This parameter may be the angle α of the lamella with the channel walls for a zigzag packing or the length L_W of the droplet perimeter in contact with the sidewall for the bamboo packing or the staircase packing. These explicit parametrizations allow us to examine the discontinuous and history-dependent transitions in the parameter region where several stable states coexist.

At low values of $\phi \leqslant \phi^* \simeq 0.8130$ we find only a single equilibrium configuration for a given channel width [see Fig. 4(a)]. This configuration may be a bamboo packing at low values of the dimensionless channel width w or a zigzag packing at large values of w, corresponding to the red line in Fig. 2(b).

For area fractions slightly above ϕ^*, a small hysteresis loop appears in the range of the zigzag packing. Note that the branch of the hysteresis loop with the highest energy corresponds to a mechanically unstable configuration in contrast to the remaining two branches. The values of the dimensionless channel width w corresponding to the lower and upper limits of the hysteresis loop are located on the lower and upper branches, respectively, of the black dotted lines in the packing diagram in Fig. 2(b). The point where the two branches of the two remaining mechanically stable solutions cross defines the transition line shown as the solid black line starting at $\mathcal{C}$ in Fig. 2(b).

Increasing the area fraction further, we observe a direct transition between packings B and Z when following the lowest, globally stable branch [see also Fig. 4(c)]. At even higher area fractions the transition occurs between B and SC, in agreement with the limit of dry emulsions $\phi \to 1$, which excludes the packing Z. At these points the black line starting at $\mathcal{C}$ in Fig. 2(b) takes over as the transition line between globally stable packings.

Interestingly, the point where the branches of the bamboo packing and the zigzag packing join coincides with the lower end point of the hysteresis loop for area fractions $\phi \gtrsim 0.9356$. Similarly, the upper end point and the point where the branch of the Z and SC packings join become identical for $\phi \gtrsim 0.9960$. Hence, in this range of area fractions close to one the zigzag packing appears only in the unstable branch of the hysteresis loop. These area fractions correspond to the points in the packing diagram in Fig. 2(b) where the dotted lines indicating the limits of metastability merge with the dashed transition lines, which indicate a continuous crossover between metastable packings.

In order to visualize the energy landscape that gives rise to the hysteresis loops depicted in Fig. 4, one needs to choose a suitable additional control parameter. Provided that such a control parameter exists, the energy landscape, or restricted energy, is given by the value of the interfacial energy of the interfacial configuration that minimizes the energy under the constraint of the additional control parameter fixed to a certain value. This implies that the restricted energy is, in the first place, a function of this additional control parameter.

The method described above allows us to determine saddle point or mountain pass configurations between two mechanically stable droplet packings that appear as local minima of the restricted energy. To resolve the energy landscape of the discontinuous transition shown in Fig. 4 we employed the freely available software package SURFACE EVOLVER [27] to find energetically minimal droplet packings under the constraint of a fixed distance of the droplet's center of mass to the centerline of the channel $Y_{\text{c.m.}}$. Experimentally, similar constraints could be enforced by an external field, such as gravity, when the droplets have different densities. The value of the interfacial energy in an energy minimum under this constraint as a function of dimensionless distance $y_{\text{c.m.}} \equiv Y_{\text{c.m.}}/W$ for given area fraction $\phi = 0.925$ is shown in Fig. 5 for a series of dimensionless channel widths w between 1.2 and 1.8, i.e., in the region of the hysteresis loop depicted in Fig. 4(c). For the sake of visibility and comparability, we

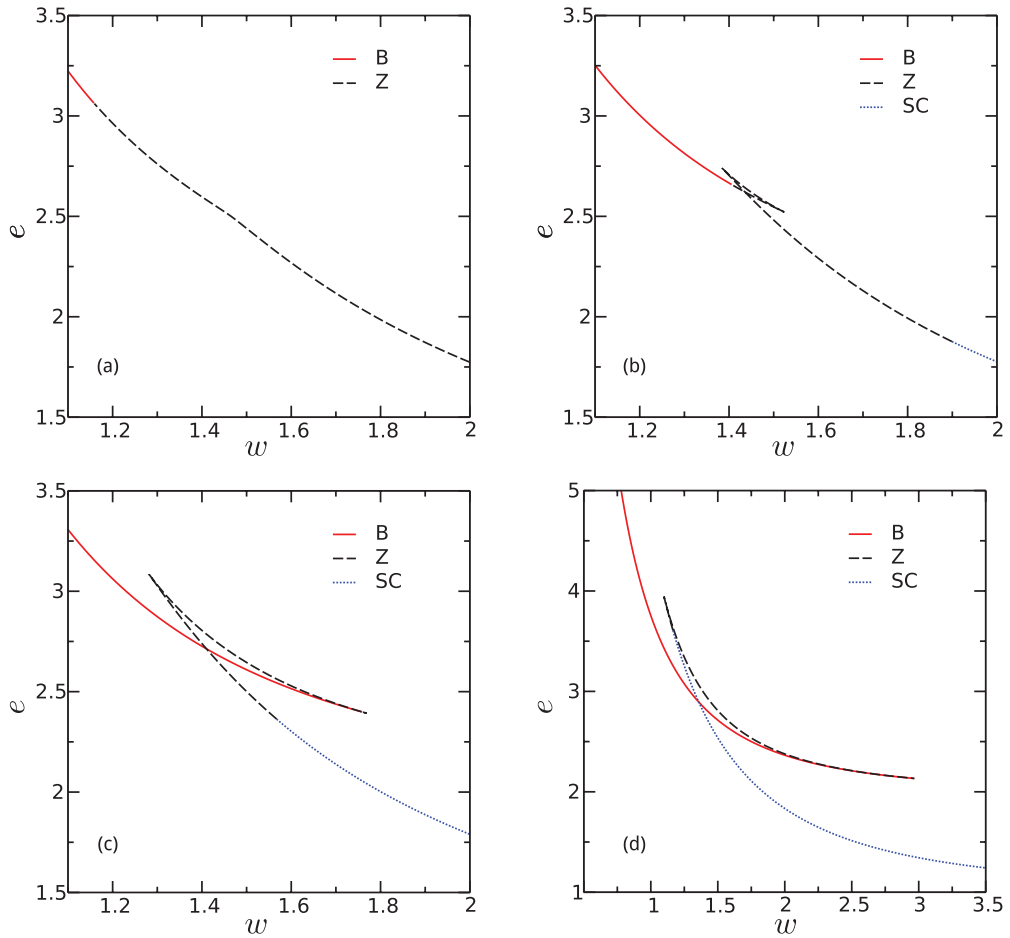

FIG. 4. (Color online) Hysteresis loop of the interfacial energy $e = E/\tau W$ of a droplet as a function of the dimensionless channel width $w = W/\sqrt{A_d}$ for area fractions (a) $\phi = 0.8$, (b) $\phi = 0.875$, (c) $\phi = 0.925$, and (d) $\phi = 0.975$. Here $\tau = \pi\gamma D/4$ is the effective line tension of the in-plane droplet contour, W is the width of the channel, A_d is the area of a droplet, and γ is the interfacial tension of the liquid-liquid interface.

subtracted for each restricted energy curve individually the value e_0 at $y_{\text{c.m.}} = 0$.

A comparison of Figs. 5 and 4 shows that the restricted interfacial energy for a given value of the dimensionless channel width and area fraction exhibits a number of extrema that matches the number of stable states seen in a corresponding vertical cut through the hysteresis loop. In the area of the loop the three coexisting states correspond to two minima and one maximum of the restricted interfacial energy, while for the top and bottom curves in Fig. 5, only one minimum can be found (a bamboo packing with completely aligned droplets at $y_{\text{c.m.}} = 0$ and a staircase packing with four neighbors, respectively). Since the intermediary nonequilibrium configurations in Fig. 5 cannot be categorized in the same way as the equilibrium configurations discussed so far, we chose to indicate only the number of direct neighbors each droplet has by the line color. When moving through the curves from top to bottom, it can be seen how the global minimum changes place between the two mechanically stable solutions and how the globally stable zigzag packing later transforms into a staircase packing with four neighbors, as also indicated in Fig. 4(c). The insets show snapshots of such unstable states corresponding to the parameter values indicated by the circles as obtained from our numerical energy minimizations. Note that these states are not mechanically stable once the additional constraint enforced by buoyancy forces is lifted, so they will not be observed in experiments with equally buoyant droplets.

V. CONCLUSION

Motivated by microfluidic experiments with monodisperse emulsions, we examined the appearance of periodic droplet packings in flat linear channels of a rectangular cross section. In this effectively two-dimensional limit the geometry and stability of static droplet packings is governed by the channel width normalized by the droplet size w and the area fraction of the dispersed phase ϕ. We restricted our considerations to packings of congruent droplets and found four different packings: slugs S, a bamboo structure B, a zigzag packing Z where each droplet has two direct neighbors, and a staircase packing SC with four neighbors. In agreement with the limit of dry, i.e., foamlike effectively two-dimensional emulsions, the transition between single- and double-row packings in a widening or narrowing channel

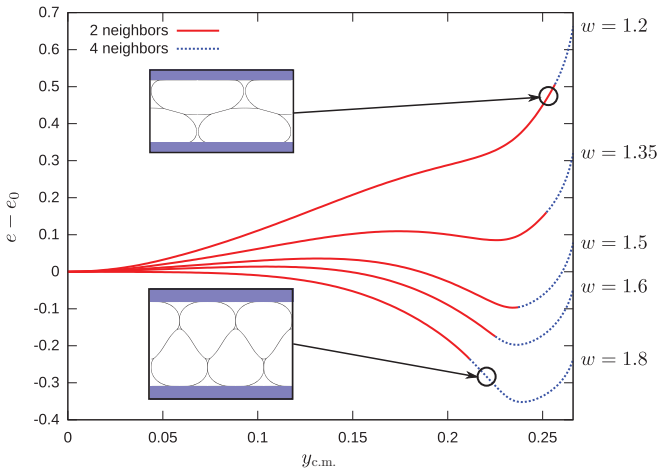

FIG. 5. (Color online) Energy landscapes of droplet packings showing the evolution of stable states when changing the channel width w. The control parameter on the abscissa is the lateral position of the droplet's center of mass $y_{\mathrm{c.m.}}$. Shown is the dimensionless restricted interfacial energy $e - e_0$ for different dimensionless channel widths w at an area fraction of $\phi = 0.925$ [thus corresponding to Fig. 4(c)]. The insets show simulation snapshots of the nonequilibrium intermediate packings indicated by the black circles. The line color encodes the number of neighbors a droplet in the corresponding packing has.

becomes increasingly hysteretic as the area fraction of the dispersed phase approaches one. The hysteresis loop shrinks to single point at $\phi = \phi^* \simeq 0.8130$ and $w = w^* \simeq 1.458$ when decreasing ϕ. The point (ϕ^*, w^*) corresponds to a bifurcation of multiple equilibria in the range of zigzag packings.

The onset of hysteresis is qualitatively consistent with works on wet foams reporting a strong increase of irreversible bubble rearrangements during shear as the area fraction of the continuous phase is decreased. The bifurcation of equilibrium packings Z can be characterized by a caustic in the space of control parameters. This caustic is located inside the bow of the jamming line between a perfect one-row and a two-row packing of circular disks. Hence it will be interesting to study the jamming and compression of monodisperse droplet packings between two-row and three-row structures. Because the corresponding transition between dry hexagonal one-row and two-row packings is apparently hysteretic, we expect to observe at least one bifurcation of equilibrium configurations. Unfortunately, the three-row packing and all higher packings consist of at least two different congruent droplet shapes. Hence the complete analytical treatment of this problem is challenging and it may be necessary to use numerical minimizations of the interfacial energy.

In this work we assumed congruent droplet packings in equilibrium. It would be interesting to extend the present analysis to noncongruent and multirow droplet packings. Garstecki and Whitesides [28,29] already enumerated a number of minimal-energy tessellations of noncongruent multirow packings in dry foams. Tessellations involving two different tiles have also been reported in Ref. [30]. It is possible that some of the structures investigated in that work are unstable with respect to transversal or longitudinal rearrangements of the droplets. In other words, the two-row packings either may break the up-down symmetry or the distribution of droplets may become heterogeneous along the channel. Calculations of the stress as a function of the area fraction at fixed droplet area indicate that instabilities of the latter type, characterized by a negative compressibility, are found in a certain range of the control parameter [15]. The results of experimental works in comparison to the numerical computations are presented in Ref. [15].

ACKNOWLEDGMENTS

The authors gratefully acknowledge stimulating discussions with Jean-Baptiste Fleury and Ralf Seemann. This work was supported by the German Science Foundation under Grant No. BR3749/1-1.

APPENDIX A: GEOMETRICAL CONSTRUCTION

As mentioned in Sec. III, certain classes of droplet packings can be constructed using elementary geometry only. In the case of bamboo packings, zigzag packings, and staircase packings, one can partition the channel into equal tiles where each tile contains exactly one droplet (see Fig. 6). These droplet shapes can be parametrized by the radius R of the curved parts of the contour and the tilt angle α of the lamellae. The droplet area a_d and the area of the continuous phase of a tile a_c can then be expressed as functions of these parameters.

1. Zigzag packing Z

To be consistent with the assumption of only two neighboring droplets we have to impose the restriction

$$\alpha \in \left[\frac{\pi}{6}, \frac{\pi}{2}\right], \quad r \in \left[0, \frac{1}{2(1+\cos\alpha)}\right] \tag{A1}$$

to the tilt angle α of the straight lamella and the dimensionless radius $r \equiv R/W$ of the circular segments. The two tilted lamellae and the part of the droplet contour in contact with the lateral walls of the channel define a triangle. For the definition of the droplet geometry see Fig. 6. The dimensionless height $h \equiv H/W$ of this fundamental triangle then reads

$$h = 1 - r\left(1 + 2\cos\alpha - \frac{1}{\cos\alpha}\right), \tag{A2}$$

so that the dimensionless area $a_d \equiv A_d/W^2$ of the droplet becomes

$$a_d = h^2 \cot\alpha - r^2\left[\cot^2\left(\frac{\alpha}{2}\right)\tan\alpha - \pi\right]. \tag{A3}$$

The dimensionless area of the tile $a_c \equiv A_c/W^2$ of the droplet occupied by the continuous phase takes the form

$$a_c = r^2[4\sin\alpha(1+\cos\alpha) - \pi]. \tag{A4}$$

In order to obtain the interfacial energy of the droplet we have to compute the total length of its contour. The boundary of a single, effectively two-dimensional droplet comprises the lamellae to both neighboring droplets, a single interface to a channel wall, and the interface to the bulk of the continuous

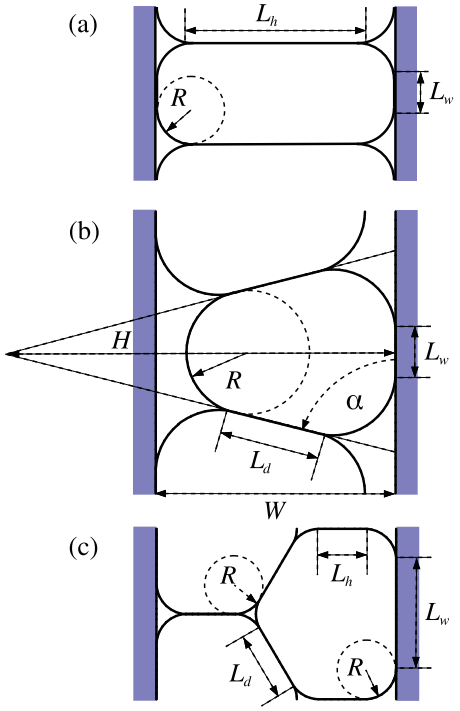

FIG. 6. (Color online) (a) Schematic of a bamboo packing (B), (b) zigzag packing (Z) with two neighboring droplets, and (c) staircase (SC) with four neighboring droplets. Here L_w is the length of the effective droplet contour in contact with the sidewall, W is the width of the channel, R is the radius of curvature of the effective droplet contour, L_d is the length of the lamella of two nearest-neighbor droplets, and L_h is the length of the lamella to the next-nearest-neighbor droplet. The triangle defined by two adjacent lamellae has a height H.

phase. We find

$$\ell_d = \frac{1 - 2r(1 + \cos\alpha)}{\sin\alpha} \tag{A5}$$

for the dimensionless length $\ell_d \equiv L_d/W$ of the interface between both neighboring droplets,

$$\ell_w = 2\left[h\cot\alpha - r\cot\left(\frac{\alpha}{2}\right)\right] \tag{A6}$$

for the dimensionless length $\ell_w \equiv L_w/W$ of the interface in contact with the lateral channel walls, and simply

$$\ell_c = 2\pi r \tag{A7}$$

for the length of the circular parts. Hence the dimensionless interfacial energy $e = E/\tau W$ of a droplet in a zigzag packing is given by

$$e = 2\,\ell_d + \ell_w + \ell_c, \tag{A8}$$

with the effective line tension τ according to Eq. (5) in Sec. II.

To determine possible equilibrium configurations in terms of the angle α and radius r at a given value of the area fraction ϕ, we have to solve a quadratic equation

$$(1 - \phi)\,a_d - \phi\,a_c = 0 \tag{A9}$$

in the radius r. It turns out that only one of the two roots of Eq. (A9) corresponds to a physically meaningful configuration. The explicit parametrization $r(\alpha,\phi)$ of this solution allows us to parametrize the interfacial energy and the channel width as a function of the tilt angle α for given values of ϕ.

APPENDIX B: BIFURCATION

Instabilities of the droplet configuration can be detected from the set of stationary configurations for given control parameters, in this case, for fixed area fraction ϕ and droplet area a_d. At low area fractions ϕ and at droplet areas close to the line where the droplets come into mutual contact and in contact with the channel walls, we find only one stationary configuration (characterized by α and r). However, at a certain threshold area fraction one observes a bifurcation into three stationary solutions, i.e., there are suddenly three droplet configurations with the same Laplace pressure and area fraction for different values of α and r. It is reasonable to assume that these solutions correspond to two local minima and one saddle point of the interfacial energy.

The point of bifurcation and the boundaries of local stability can be obtained from the Jacobian

$$J(\alpha,r) = \begin{pmatrix} \partial_r a_d(\alpha,r) & \partial_\alpha a_d(\alpha,r) \\ \partial_r a_c(\alpha,r) & \partial_\alpha a_c(\alpha,r) \end{pmatrix} \tag{B1}$$

of the map between the order parameters (α,r) and the control parameters (a_d,a_c). The Jacobian becomes singular for $|J(\alpha,r)| = 0$, which implicitly defines the function

$$r_b(\alpha) = \frac{\sec^2(\alpha/2)[4\sin\alpha + 2\sin(2\alpha) - \pi]}{\pi[\cos(2\alpha) - 2\cos\alpha] + 3\sin(2\alpha) - 6\sin\alpha}. \tag{B2}$$

Mapping the solution $r_b(\alpha)$ back onto the space of the control parameters area fraction and droplet area yields a parametric curve $[a_d(\alpha),\phi(\alpha)]$ in the packing diagram in Fig. 2(b). In the generic case, a point on the curve corresponds to values of the control parameters where the number of stationary configurations changes by 2, i.e., while approaching this line a local minimum and a saddle point of the energy approach and disappear on the line. At the cusp at $\phi^* \simeq 0.8130$ and $a^* \simeq 0.4707$, or dimensionless channel width $w^* = 1/\sqrt{a^*} \simeq 1.4576$, one observes a bifurcation of a single local minimum of the interfacial energy into a saddle point and two local minima.

[1] C. Priest, S. Herminghaus, and R. Seemann, Appl. Phys. Lett. **88**, 024106 (2006).
[2] G. F. Christopher and S. L. Anna, J. Phys. D **40**, R319 (2007).
[3] J.-C. Baret, F. Kleinschmidt, A. El Harrak, and A. D. Griffiths, Langmuir **25**, 6088 (2009).
[4] A. B. Subramaniam, M. Abkarian, and H. A. Stone, Nature Mater. **4**, 553 (2005).
[5] W. B. Weibel and G. M. Whitesides, Curr. Opin. Chem. Biol. **10**, 584 (2006).
[6] S. Holtze *et al.*, Lab Chip **10**, 1632 (2008).

[7] V. Chokkalingam *et al*., Chem. Phys. Chem. **11**, 2091 (2010).
[8] C. Priest, S. Herminghaus, and R. Seemann, Appl. Phys. Lett. **89**, 134101 (2006).
[9] K. Ahn, C. Kerbage, T. P. Hunt, D. R. Link, and D. A. Weitz, Appl. Phys. Lett. **88**, 024104 (2006).
[10] S. Thutupalli, R. Seemann, and S. Herminghaus, Soft Matter **7**, 1312 (2011).
[11] S. A. Vanapalli, C. R. Iacovella, K. E. Sung, D. Mukhija, J. M. Millunchick, M. A. Burns, S. C. Glotzer, and M. J. Solomon, Langmuir **24**, 3661 (2008).
[12] L. Shui, S. E. Kooij, D. Wijnperle, A. van Den Berg, and J. C. T. Eijkel, Soft Matter **5**, 2708 (2009).
[13] R. Mehrotra, N. Jing, and J. Kameoka, Appl. Phys. Lett. **92**, 213109 (2008).
[14] E. Surenjav, C. Priest, S. Herminghaus, and R. Seemann, Lab Chip **9**, 325 (2009).
[15] J.-B. Fleury, O. Claussen, M. Brinkmann, and R. Seemann, Appl. Phys. Lett. **99**, 244104 (2011).
[16] W. Drenckhan, S. Cox, G. Delaney, H. Holste, D. Weaire, and N. Kern, Colloids Surf. A **263**, 52 (2005).
[17] J.-P. Raven and P. Marmottant, Phys. Rev. Lett. **102**, 084501 (2009).
[18] N. Kern, D. Weaire, A. Martin, S. Hutzler, and S. J. Cox, Phys. Rev. E **70**, 041411 (2004).
[19] D. Reinelt, P. Boltenhagen, and N. Rivier, Eur. Phys. J. E **4**, 299 (2001).
[20] S. Hutzler, J. Barry, P. Grasland-Mongrain, D. Smyth, and D. Weaire, Colloids Surf. A **344**, 37 (2009).
[21] P. Marmottant and J.-P. Raven, Soft Matter **5**, 3385 (2009).
[22] M. Brinkmann, J. Kierfeld, and R. Lipowsky, J. Phys. A **37**, 11547 (2004).
[23] M. Brinkmann, J. Kierfeld, and R. Lipowsky, J. Phys.: Condens. Matter **17**, 2349 (2005).
[24] J. Molnar, Acta Math. Hungar. **31**, 173 (1978).
[25] Z. F. Füredi, Discrete Comput. Geom. **6**, 95 (1991).
[26] M. A. Fortes, M. E. Rosa, M. F. Vaz, and P. I. C. Teixeira, Eur. Phys. J. E **15**, 395 (2004).
[27] K. Brakke, Exp. Math. **1**, 141 (1992).
[28] P. Garstecki, I. Gitlin, W. DiLuzio, G. M. Whitesides, E. Kumacheva, and H. A. Stone, Appl. Phys. Lett. **85**, 2649 (2004).
[29] P. Garstecki and G. M. Whitesides, Phys. Rev. E **73**, 031603 (2006).
[30] M. A. Fortes and P. I. C. Teixeira, Eur. Phys. J. E **6**, 133 (2001).